Journal of Organometallic Chemistry, 377 (1989) 291–303
Elsevier Sequoia S.A., Lausanne – Printed in The Netherlands
JOM 20168

Anionic trimetallic compounds containing Fe–E–M skeletons (E = Zn, Cd, Hg; M = Fe, Mo, W). Crystal structure of $[N(PPh_3)_2]_2[(OC)_4Fe–Hg–Fe(CO)_4]$

Santiago Alvarez *, Montserrat Ferrer, Roser Reina, Oriol Rossell *, Miquel Seco

Departament de Química Inorgànica, Facultat de Química, Universitat de Barcelona, Diagonal 647, 08028 (Spain)

and Xavier Solans

Departament de Cristal.lografia, Facultat de Geologia, Universitat de Barcelona, Martí i Franqués s/n, 08028 Barcelona (Spain)

(Received June 7th, 1989)

Abstract

Dichlorides of group 12 elements react with $(NEt_4)[HFe(CO)_4]$ in tetrahydrofuran to give the di-hydrides $[(OC)_4HFe–E–FeH(CO)_4]$ (E = Zn, Cd, Hg) in good yields. These compounds undergo proton abstraction by ^nBuLi to give di-anions $[(OC)_4Fe–E–Fe(CO)_4]^{2-}$, stabilized as their bis(triphenylphosphine)nitrogen(+) (PPN^+) salts. $(PPN)_2[(OC)_4Fe–Hg–Fe(CO)_4]$ crystallizes in the triclinic system, space group $P\bar{1}$ with a 20.382(3), b 15.328(2), and c 13.420(2) Å; α 115.96(3), β 108.89(2), and γ 87.09(2)°, and $Z = 2$. The anion consists of an almost linear spine (Fe–Hg–Fe angle 178.7(1)°), with an average Fe–Hg bond distance of 2.546(2) Å. The Fe atoms display a trigonal bipyramidal geometry, and the equatorial CO groups linked to the iron atoms are in an eclipsed conformation, resulting in an idealized D_{3h} symmetry. The existence of two conformers for this anion and the presence of Hg ··· CO backbonding are discussed on the basis of qualitative molecular orbital theory. The $[(OC)_4Fe–Hg–Fe(CO)_4]^{2-}$ anion undergoes redistribution reactions with $[M(CO)_3(\eta\text{-}C_5H_5)]_2Hg$ (M = Mo, W) to give the new unsymmetrical anions $[(OC)_4Fe–Hg–M(CO)_3(\eta\text{-}C_5H_5)]^-$.

Introduction

The chemistry of anionic trimetallic compounds containing metal–metal bonds between group 12 metals atoms and transition metals is not well documented. To the best of our knowledge, the only examples reported are the salts of the $[(OC)_4Fe–E–Fe(C0)_4]^{2-}$ anions (E = Zn, Cd, Hg) [1,2]. These derivatives were

0022-328X/89/$03.50

obtained by long and tedious synthetic procedures. In addition, some of their spectroscopic parameters are not consistent with the X-ray structures. We decided to seek to clarify this situation and to devise a new, easy and high-yield preparation method for these anions. We have also investigated their potential use as precursors of polynuclear metal-metal bonded complexes.

Results and discussion

Preparation and characterization of complexes

The new synthetic method for the preparation of the di-anions $[(OC)_4Fe–E–Fe(CO)_4]^{2-}$ involves the following steps:

(i) Preparation of the new di-hydrido compounds $[(OC)_4HFe–E–FeH(CO)_4]$ (**1a**: E = Zn; **1b**: E = Cd; **1c**: E = Hg) according to eq. 1:

$$2\ (NEt_4)[HFe(CO)_4] + ECl_2 \xrightarrow{THF} [(OC)_4HFe–E–FeH(CO)_4] + 2\ NEt_4Cl \quad (1)$$

(ii) Proton abstraction from **1(a–c)** by ^nBuLi to give the dianions $[(OC)_4Fe–E–Fe(CO)_4]^{2-}$ (**2a**: E = Zn; **2b**: E = Cd; **2c**: E = Hg), followed by precipitation as their PPN^+ salts (PPN^+ = bis(triphenylphosphine)nitrogen(+1)) (eq. 2):

$$[(OC)_4HFe–E–FeH(CO)_4] + 2\ ^nBuLi \xrightarrow{PPN^+}$$

$$(PPN)_2[(OC)_4Fe–E–Fe(CO)_4] + 2\ BuH + 2\ Li^+ \quad (2)$$

The yields of the first step are almost quantitative. Although **1a** and **1b** are thermally very unstable, **1c** can be manipulated in the air for a short time. The dianions **2** are easily isolated with yields of about 90% by addition of $(PPN^+)Cl^-$ to their THF solutions, and can be converted to **1** by protonation with trifluoroacetic acid. The $(PPN)_2$[**2**] compounds are yellow microcrystalline solids, soluble in polar solvents. They are stable under nitrogen.

Our synthetic route takes advantage of the high reactivity of the $HFe(CO)_4$ fragment towards H^+ abstraction, a property elegantly demonstrated by Darensbourg [3], and is a significant improvement on the two previously reported syntheses. Our method provides clean high-yield synthesis, which is rare for complexes of this type. Formally, complexes **1** can be viewed as the result of a Group 12 metal insertion into the Fe–Fe bond of $[(CO)_4HFe–FeH(CO)_4]$. In connection with this point, of interest is the increase of the thermal stability of **1c** compared with that of the iron dihydride, which was not stable above −80 °C [4].

The solution infrared spectra of the (PPN) salts of **2a**, **2b** and **2c** in THF in the ν(CO) region are similar, but clearly different from those reported for $[Na\{THF\}_2]_2$[**2**] (THF = tetrahydrofuran) [2], since the spectra of the latter showed a decrease in the number of well resolved bands with increasing metal size. This was attributed to the distortion of the tetracarbonyliron groups from an ideal trigonal–bipyramidal arrangement, the distortion increasing as the size of the central atom decreases [2]. Another point of interest is that all spectra show low-frequency carbonyl stretching bands, as expected for complexes with negative charge on the metal atoms.

The oxidation state of iron in $(PPN)_2$[**2b,c**] was assessed by means of ^{57}Fe Mössbauer spectroscopy (Fig. 1). The spectra of the two compounds are very

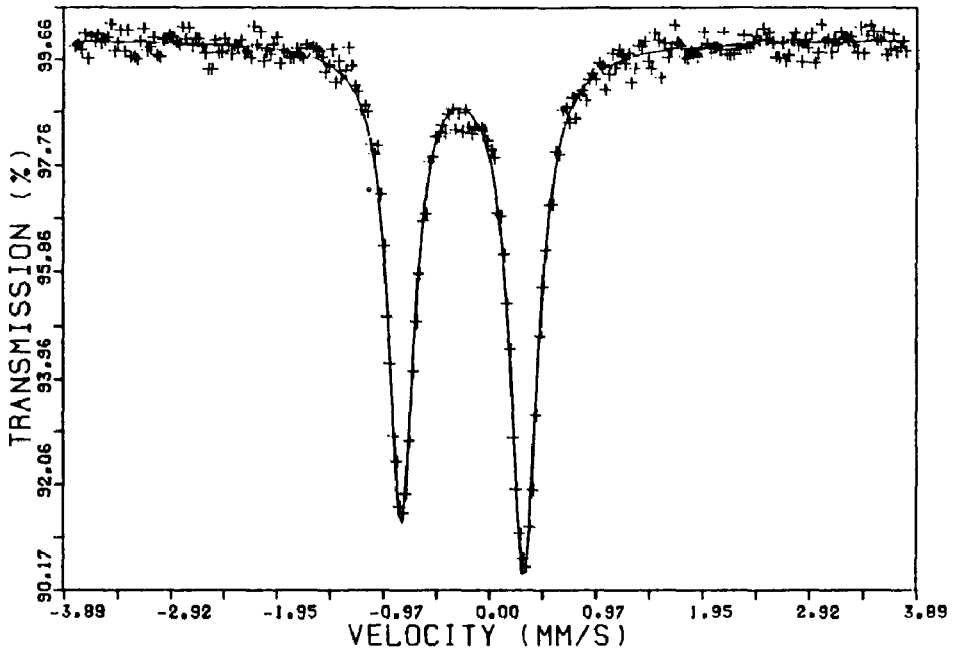

Fig. 1. Mössbauer spectrum of $(PPN)_2$[**2b**].

similar, displaying the expected quadrupole doublet. The isomer shifts at 80 K (about -0.10 mm s^{-1}) correspond approximately by a -1 charge, as found for the closely related $(NEt_4)_2[Fe_2(CO)_8]$ [5]. On the other hand, the quadrupole splitting (1.3 mm s^{-1}) is smaller than expected for five coordination, probably owing to the local C_{3v} symmetry around the iron atoms imposed by the semibridging nature of the equatorial carbonyls. Surprisingly, it was previously reported that the ^{57}Fe Mössbauer spectrum of $[Na\{THF\}_2]_2$[**2b**] shows three peaks [2], and this was unsatisfactorily explained in terms of two non-equivalent iron atoms. In our opinion, the spectrum could be that of a mixture of $[Na\{THF\}_2]_2$[**2b**] and some decomposition product arising from the poor ability of the $[Na\{THF\}_2]^+$ cation to stabilize negative species. The large volume of the PPN^+ cation, on the other hand, enhances the stability of our compounds, allowing us to record the Mössbauer spectra of pure samples. Again, we believe that unwanted decomposition products are responsible for the above differences in the IR spectra of the $[Na\{THF\}_2]_2$[**2**] compounds. This view is supported by the fact that, after exposure to air for a short period of time, the complexes described here display IR patterns similar to those previously reported.

In order to confirm the structure of these anions an X-ray crystallographic study of $(PPN)_2[(OC)_4Fe-Hg-Fe(CO)_4]$ was carried out. The crystal contains well separated $(PPN)^+$ and $[(OC)_4Fe-Hg-Fe(CO)_4]^{2-}$ ions, without short interionic contacts. Selected bond lengths and angles are listed in Table 1, and the structure of the anion is shown in Fig. 2. The anion has a practically linear Fe–Hg–Fe backbone ($\beta = 178.7(1)°$). The average Fe–Hg bond distance of 2.546(2) Å, agrees well with those in the related structures $[Na\{THF\}_2]_2$[**2c**] (2.522 Å) [2], $[Hg\{Fe(CO)_2(NO)(PEt_3)_2\}_2]$ (2.534 Å) [6], $[Hg\{Fe(CO)_2(\eta\text{-}C_5H_5)\}\{Co(CO)_4\}]$ (2.49 Å) [7], and $[(BrHg)_2Fe(CO)_4]$ (2.59 Å) [8]. The Fe atoms display a trigonal-bipyramidal geom-

Table 1

Selected interatomic distances (Å) and angles (°) for the $[(OC)_4Fe-Hg-Fe(CO)_4]^{2-}$ anion, with estimated standard deviations in parenthesis

Fe(1)–Hg	2.547(2)
Fe(2)–Hg	2.545(2)
Fe(1)–C(11)	1.782(17)
Fe(1)–C(12)	1.744(14)
Fe(1)–C(13)	1.758(12)
Fe(1)–C(14)	1.742(18)
Fe(2)–C(21)	1.700(17)
Fe(2)–C(22)	1.734(15)
Fe(2)–C(23)	1.737(20)
Fe(2)–C(24)	1.782(12)
Fe(1)–Hg–Fe(2)	178.7(1)
Hg–Fe(1)–C(11)	84.1(4)
Hg–Fe(1)–C(12)	77.8(4)
Hg–Fe(1)–C(13)	173.3(4)
Hg–Fe(1)–C(14)	84.0(4)
Hg–Fe(2)–C(21)	83.5(4)
Hg–Fe(2)–C(22)	84.6(4)
Hg–Fe(2)–C(23)	76.9(4)
Hg–Fe(2)–C(24)	173.6(4)
C(11)–Fe(1)–C(12)	121.8(8)
C(11)–Fe(1)–C(13)	99.6(7)
C(12)–Fe(1)–C(13)	95.5(6)
C(11)–Fe(1)–C(14)	109.9(7)
C(12)–Fe(1)–C(14)	122.2(8)
C(13)–Fe(1)–C(14)	99.8(7)
C(21)–Fe(2)–C(22)	110.5(7)
C(21)–Fe(2)–C(23)	121.9(7)
C(22)–Fe(2)–C(23)	121.1(9)
C(21)–Fe(2)–C(24)	100.2(7)
C(22)–Fe(2)–C(24)	98.9(6)
C(23)–Fe(2)–C(24)	96.7(6)

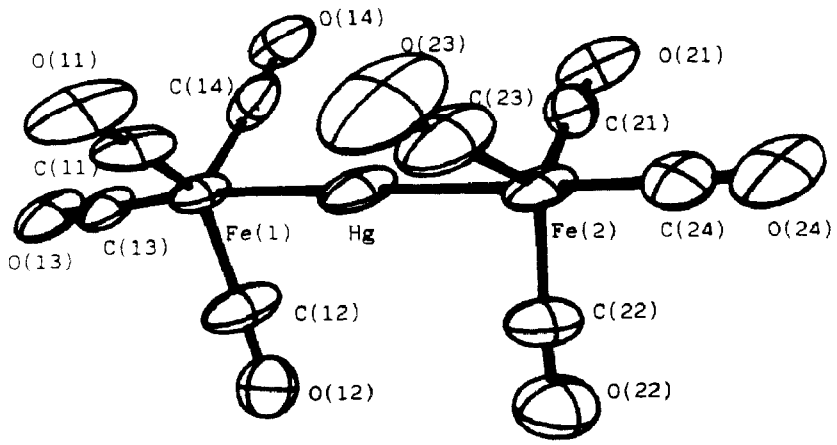

Fig. 2. Molecular structure of the anion **2c**.

etry, and the equatorial CO groups linked to the iron atoms are in an eclipsed conformation, resulting in an idealized D_{3h} symmetry. This structural feature is unique, since a staggered conformation (D_{3d} symmetry) was found for the isoelectronic complexes: $[Na\{THF\}_2]_2$[**2c**] [2], $[Hg\{Co(CO)_4\}_2]$ [9], $[Zn\{Co(CO)_4\}_2]$ [10] and [PPN][$Au\{Co(CO)_4\}_2$] [11].

Another interesting aspect of the structure is the appreciable bending of the equatorial carbonyl groups towards the mercury atom (mean Hg–Fe–C angle,

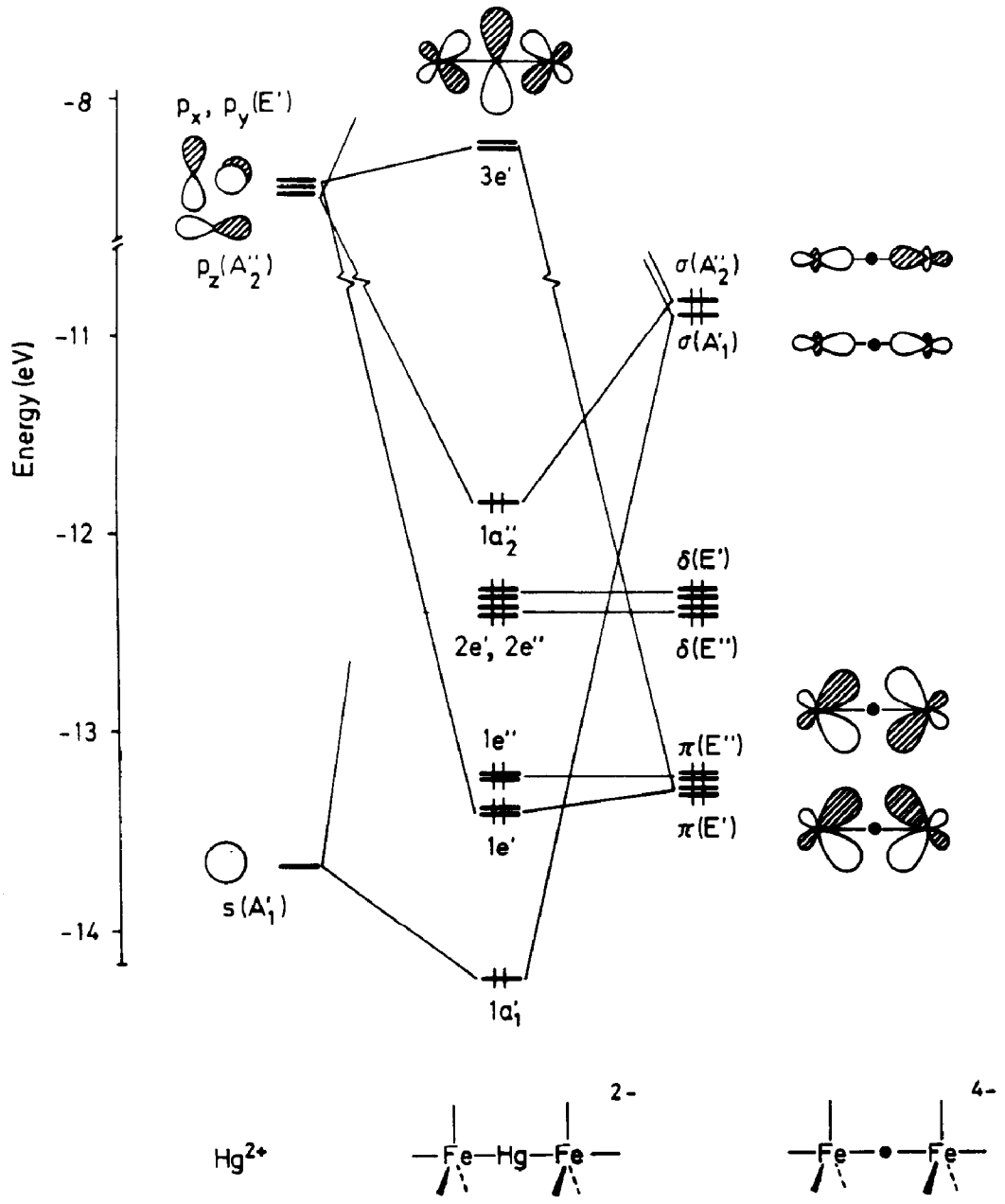

Fig. 3. Interaction diagram for Hg^{2+} and two $[Fe(CO)_4]^{2-}$ ions in a linear array with eclipsed conformation. The same diagram results for a staggered conformation.

$\alpha = 82(3)°$). A noticeable tilting of the equatorial carbonyls on trigonal–bipyramidal metals towards the main-group atom has also been described for other complexes, and is present in several thallium–iron clusters obtained recently by Whitmire et al. [12].

Electronic structure and bonding

The existence of eclipsed and staggered conformers as well as the tilting of the equatorial carbonyl groups towards the mercury atom merit qualitative theoretical analysis. Although an account of the bonding in the isoelectronic compound $[(OC)_4Co–Zn–Co(CO)_4]$ has been previously given by Silvestre and Albright [13], a brief description of the electronic structure of **2c** is needed in order to explain both structural features.

The essentials of the electronic structure of **2c** are summarized in Fig. 3, where the interaction between the central element Hg and the two external fragments $Fe(CO)_4$ is shown for an idealized eclipsed geometry ($\alpha = 90°$ and $\beta = 180°$). The orbitals of the $\{Fe(CO)_4\}_2$ fragment are just the in-phase and out-of-phase combinations of those of a pyramidal $Fe(CO)_4$ unit [14]. The $1a_1'$ and $1a_2''$ molecular orbitals are σ-bonding combinations of the trimetallic spine. There is a degenerate pair of $1e'$ molecular orbitals with some Fe–Hg π-bonding character.

It must be stressed that the $1e'(\pi)$ orbitals (Fig. 3) are degenerate, and consequently insensitive to internal rotations around the Fe–Hg–Fe backbone. Thus no electronic barrier to internal rotation should be expected for this compound, and so the presence of both conformers must be related to the packing forces in the crystal.

Another interesting structural aspect is the tendency of the equatorial carbonyl groups to adopt a semibridging situation (i.e., $\alpha < 90°$). In a recent structural analysis of semibridging carbonyls, Crabtree and Lavin [15] found no clear trend for

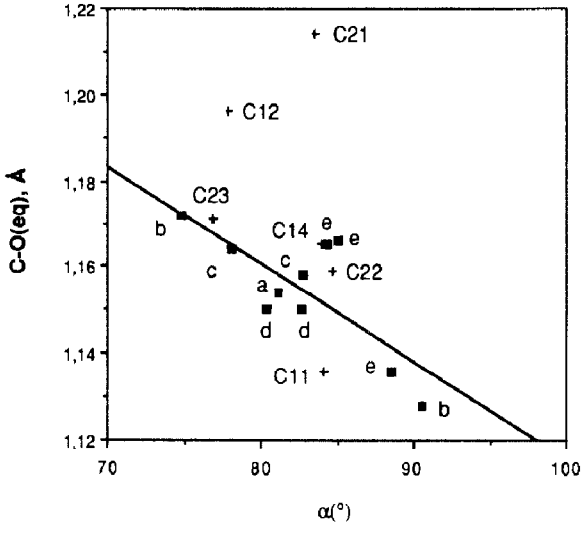

Fig. 4. Equatorial CO bond distances as a function of the M–E–CO angle α, for several compounds reported in the literature (filled squares), together with the data for compound $(PPN)_2[(OC)_4Fe–Hg–Fe(CO)_4]$ (crosses). The following M–E pairs are included in the plot: Zn–Co (point a: ref. 10), Zn–Fe (b: ref. 28, and c: ref. 2), Fe–Hg (d: ref. 29, and e: ref. 6).

bonds between transition metal and main group elements, suggesting that the main group element cannot donate electrons efficiently to the CO π system. Nevertheless, in the carbonyl transition metal-main group element compounds, the equatorial CO ligands of the transition metal are always bent towards the main group element, revealing the presence of some electronic interaction. Our calculations indicate that the most stable structure for **2c** corresponds to $\alpha \approx 78°$ when all the equatorial carbonyls are bent simultaneously in the eclipsed conformation. Formally one can describe this interaction as a donation of electron density from the M–E–M σ bonds towards π^*_{CO}, and it can be expected that the degree of bending should have some influence on the strengths of both the equatorial CO groups and M–E bonds: for smaller values of α, a larger donation would result in an increased population of π^*_{CO} and a decreased population of the σ orbitals of the backbone, and hence larger CO and ME bond lengths. In Fig. 4 we show a plot of the CO bond distances as a function of α for several M–E compounds, taken from the literature (closed squares), together with the data for $(PPN)_2$[**2c**] (crosses). The data from the literature show the expected trend. From the six independent equatorial CO bond distances of the present structure, only two deviate from the general behavior. A glance at the thermal parameters shows that the distances which deviate correspond to ill localized carbon or oxygen atoms.

Reactivity of the dianionic trinuclear complexes

Once the structure of $(PPN)_2$[**2c**] was established, it seemed of interest to examine its potential use in double exchange processes and in ligand substitution reactions. Processes of the first type between symmetrical mercury species, M–Hg–M and M′–Hg–M′ have been previously reported [16–18], although the factors which drive the equilibrium towards unsymmetrical species are not yet clear. As an extension of this synthetic method to anionic trimetallic mercury compounds, $[M–Hg–M']^-$, we treated $(PPN)_2$[**2c**] with $[(\eta\text{-}C_5H_5)(OC)_3M–Hg–M(CO)_3(\eta\text{-}C_5H_5)]$ (M = Mo, W) in THF. Unsymmetrical mercury complexes (**3**, M = Mo; **4**, M = W) were formed in good yields immediately upon mixing, as shown in eq. 3:

$$(PPN)_2[(OC)_4Fe–Hg–Fe(CO)_4] + [(\eta\text{-}C_5H_5)(OC)_3M–Hg–M(CO)_3(\eta\text{-}C_5H_5)] \rightarrow 2(PPN)[(OC)_4Fe–Hg–M(CO)_3(\eta\text{-}C_5H_5)] \quad (3)$$

Compounds **3** and **4** are the first anionic mercury complexes containing an asymmetric M–Hg–M′ array. They are yellow crystalline solids and were characterized by microanalyses and IR and ^1H spectra. The complex ν(CO) IR bands for **3** and **4** are practically identical, indicating that they must have similar structures. Both complexes can be stored under nitrogen for a long time without appreciable decomposition. In contrast with the reactions represented by eq. 3, treatment of $(PPN)_2$[**2a–b**] with $[(\eta\text{-}C_5H_5)(OC)_3Mo]_2E$ under the same conditions does not produce the corresponding trinuclear complexes $(PPN)[(OC)_4Fe–E–Mo(CO)_3(\eta\text{-}C_5H_5)]$ (E = Zn, Cd), and the reagents are recovered unaltered after several hours. Analogously, no reaction is observed between [**1a–c**] and $[(\eta\text{-}C_5H_5)(OC)_3Mo]_2E$. The reasons for this reactivity difference are currently under investigation.

The nucleophilicity of $(PPN)_2$[**2c**] in ligand substitution reactions has been explored in order to evaluate its potential use to form long metallic chains. $(PPN)_2$[**2c**] was allowed to react with $ClAu(PPh_3)$ in THF and the major product

was the known trimetallic cluster $[(OC)_4Fe\{Au(PPh_3)\}_2]$, the minor products were not investigated. The products indicated that a metallic chain fragmentation occurs followed by a reorganization of the residual moieties to give the gold cluster. This behavior is in good agreement with the accepted idea that long metallic chains tend to break up to give mixtures of compounds with fewer metal atoms, as recently shown by Stone [19].

In a second reaction, treatment of $(PPN)_2$[**2c**] with $ClHg(C_6Cl_5)$ in THF immediately gives $Hg(C_6Cl_5)_2$ and the polymeric insoluble $[Hg\{Fe(CO)_4\}]_x$ as indicated by their IR spectra. This transformation is easily interpreted in terms of ligands redistribution of the unstable $[(C_6Cl_5)Hg-Fe(CO)_4-Hg-Fe(CO)_4-Hg-(C_6Cl_5)]$ in the light of our results on bimetallic mercury transition metal compounds [20]. In spite of the unsuccessful outcome, we think that under appropriate conditions $(PPN)_2$[**2c**] could be an excellent starting material for forming chains longer than the usually reported three-membered ones. Further studies in this area are in progress.

Experimental

Solvents were dried by standard methods, and all manipulations and reactions were performed in Schlenk-type flasks under nitrogen. Elemental analyses for C, H, and N, were carried out at the Institut de Bio-Orgànica de Barcelona. The ^1H NMR spectra were recorded on a Bruker WP 80SY spectrometer; ^1H shifts are relative to $Si(CH_3)_4$. Infrared spectra were recorded on a Perkin–Elmer 1330 spectrophotometer. Mössbauer spectra were recorded using a 20 mCi of ^{57}Co source in a Rh matrix, and the calibration was with iron foil. No appreciable changes in the Mössbauer spectra were detected upon increasing the temperature. Compounds $(NEt_4)[HFe(CO)_4]$ [21] and $[(\eta\text{-}C_5H_5)(OC)_3M-Hg-M(CO)_3(\eta\text{-}C_5H_5)]$ [17] were prepared by procedures described previously.

*Synthesis of $[(OC)_4HFe-Hg-FeH(CO)_4]$ (**1c**)*

Solid $HgCl_2$ (1.08 g, 4.0 mmol) was added to a suspension of $(NEt_4)[HFe(CO)_4]$ (2.0 g, 6.7 mmol) in THF (100 ml), the mixture turning yellow immediately. After 2 h stirring, the solution was allowed to warm to 0 °C, and at this point the salts were filtered off and solvent was evaporated under reduced pressure until microcrystals were deposited. A second crop of crystals was obtained by addition of n-hexane to the mother liquor. Yield: 1.7 g (94%). Compounds **1a** and **1b** were prepared analogously and used in situ. IR (THF, cm^{-1}) for **1a**: 2015s, 1930(s,br); for **1b**: 2010s, 1930(s,br); for **1c**: 2019s, 1950(s,br). Anal. Found: C, 17.52; H, 0.41. **1c** calc: C, 17.84; H, 0.36%.

*Preparation of $(PPN)_2[(OC)_4Fe-Hg-Fe(CO)_4]$ (**2c**)*

Butyllithium was slowly added dropwise from a syringe to a solution of $[(OC)_4HFe-Hg-FeH(CO)_4]$ (0.8 g, 1.48 mmol) in THF (40 ml) at −78 °C until a cream suspension was obtained and no further gas bubbles were evolved upon addition of more BuLi. Then 1.66 g (2.9 mmol) of PPN^+Cl^- were added, and the mixture was stirred for 8 h, during which lemon-yellow microcrystals of the dianion separated. These were filtered off, washed with hexane, dried in vacuo, and recrystallized from an acetone-methanol mixture. Yield: 2.18 g, 91%. $(PPN)_2$[**2a**]

Table 2

Final positional coordinates ($\times 10^4$) and equivalent thermal parameters for non-hydrogen atoms of $(PPN)_2$[**2c**] (estimated standard deviations in parenthesis)

Atom	x	y	z	B_{eq}
Hg	25002(3)	25000(4)	45024(5)	4.51(3)
Fe(1)	36628(8)	35681(12)	55955(15)	3.64(8)
Fe(2)	13391(8)	14326(12)	33667(15)	3.61(9)
P(11)	6879(1)	3701(2)	8985(3)	2.97(13)
N(1)	7651(4)	3636(6)	9727(7)	2.98(41)
P(12)	8422(1)	4027(2)	9979(3)	3.01(13)
P(21)	8119(1)	1300(2)	3406(3)	2.87(13)
N(2)	7354(4)	1355(6)	3434(7)	3.14(41)
P(22)	6577(1)	970(2)	2531(3)	3.10(14)
C(11)	3181(6)	4426(11)	5172(12)	4.90(74)
O(11)	2908(5)	5030(8)	4985(10)	7.26(66)
C(12)	3873(6)	2511(12)	4580(12)	5.23(77)
O(12)	4031(6)	1802(8)	3881(10)	8.95(64)
C(13)	4505(7)	4192(8)	6243(11)	4.26(63)
O(13)	5063(5)	4615(7)	6716(9)	5.92(51)
C(14)	3531(8)	3624(9)	6840(12)	5.44(73)
O(14)	3460(5)	3733(6)	7714(8)	6.14(56)
C(21)	1464(6)	1385(9)	4656(11)	4.33(59)
O(21)	1546(5)	1286(7)	5537(9)	6.47(57)
C(22)	1804(7)	596(11)	2575(12)	4.73(74)
O(22)	2076(5)	−27(8)	2037(9)	7.12(61)
C(23)	1148(7)	2493(12)	3210(14)	5.94(85)
O(23)	965(5)	3173(9)	3053(12)	9.62(81)
C(24)	488(7)	794(9)	2537(12)	4.33(67)
O(24)	−67(5)	406(7)	2045(9)	6.19(53)
C(101)	6583(5)	2632(8)	7604(10)	3.15(54)
C(102)	6955(6)	1816(9)	7426(11)	4.02(64)
C(103)	6690(7)	946(9)	6427(11)	4.83(70)
C(104)	6044(8)	894(11)	5612(12)	6.09(81)
C(105)	5697(7)	1707(12)	5761(13)	6.18(86)
C(106)	5946(6)	2551(9)	6724(10)	4.83(63)
C(111)	6321(6)	3755(7)	9784(10)	2.88(55)
C(112)	6585(7)	3750(8)	10866(12)	4.50(69)
C(113)	6134(8)	3833(8)	11488(11)	4.75(74)
C(114)	5414(8)	3847(9)	10961(15)	5.18(82)
C(115)	5144(7)	3855(10)	9886(14)	5.80(81)
C(116)	5597(6)	3810(9)	9315(12)	4.66(67)
C(121)	6780(5)	4766(8)	8716(10)	3.30(56)
C(122)	6828(6)	4738(10)	7712(11)	4.46(71)
C(123)	6808(6)	5660(13)	7675(14)	5.62(90)
C(124)	6767(7)	6511(11)	8596(16)	5.88(89)
C(125)	6697(7)	6504(10)	9548(14)	5.60(81)
C(126)	6705(6)	5608(9)	9630(12)	4.49(69)
C(201)	8502(5)	4390(8)	8910(10)	3.51(58)
C(202)	8657(6)	5354(9)	9188(12)	4.61(67)
C(203)	8372(6)	3872(10)	6886(12)	5.12(76)
C(204)	8653(6)	5570(11)	8279(14)	5.02(82)
C(205)	8522(6)	4851(11)	7134(13)	5.13(75)
C(206)	8372(6)	3675(8)	7763(10)	3.72(58)
C(211)	8757(5)	5054(7)	11410(9)	3.35(52)
C(212)	8285(6)	5544(8)	11979(10)	4.15(60)
C(213)	8526(7)	6305(9)	13072(11)	5.11(70)

Table 2 (continued)

Atom	x	y	z	B_{eq}
C(214)	9256(7)	6599(9)	13656(12)	5.54(72)
C(215)	9726(6)	6117(9)	13110(12)	5.66(70)
C(216)	9470(6)	5318(9)	11966(10)	4.73(62)
C(221)	8977(5)	3083(8)	9987(9)	3.33(52)
C(222)	9580(6)	3044(9)	9720(10)	4.13(61)
C(223)	10026(6)	2353(10)	9795(11)	5.06(68)
C(224)	9851(8)	1663(10)	10087(12)	5.68(76)
C(225)	9246(7)	1678(10)	10329(12)	5.85(78)
C(226)	8800(7)	2371(9)	10266(11)	4.66(67)
C(301)	6237(6)	−50(8)	2604(9)	3.27(54)
C(302)	6729(6)	−525(8)	3163(10)	4.23(62)
C(303)	6443(8)	−1310(10)	3217(13)	6.20(84)
C(304)	5738(6)	−1595(9)	2799(12)	5.41(70)
C(305)	5273(6)	−1113(9)	2246(12)	5.39(67)
C(306)	5522(6)	−347(9)	2129(11)	4.88(65)
C(311)	6031(5)	1929(7)	2927(10)	3.01(52)
C(312)	5419(6)	1925(9)	2060(12)	4.32(66)
C(313)	4984(7)	2634(10)	2390(14)	5.46(80)
C(314)	5138(7)	3325(10)	3560(15)	5.35(82)
C(315)	5747(7)	3335(10)	4395(13)	5.60(79)
C(316)	6195(6)	2619(9)	4060(11)	4.17(65)
C(321)	6493(5)	623(7)	1040(9)	3.25(47)
C(322)	6631(6)	1326(8)	735(10)	3.64(59)
C(323)	6609(7)	1116(10)	−365(12)	5.29(73)
C(324)	6477(6)	150(11)	−1222(11)	5.07(72)
C(325)	6340(6)	−574(10)	−938(11)	4.84(70)
C(326)	6342(5)	−339(9)	171(11)	4.11(62)
C(401)	8419(5)	2376(7)	3392(9)	3.32(53)
C(402)	8040(6)	3179(9)	3672(11)	4.46(64)
C(403)	8316(7)	4065(9)	3796(11)	5.21(72)
C(404)	8944(7)	4112(10)	3640(12)	5.69(80)
C(405)	9305(7)	3312(11)	3360(13)	5.94(80)
C(406)	9076(6)	2433(9)	3222(11)	4.76(65)
C(411)	8223(5)	234(8)	2191(9)	3.08(54)
C(412)	8180(6)	226(9)	1156(10)	4.17(62)
C(413)	8202(6)	−626(12)	203(11)	5.56(75)
C(414)	8240(7)	−1527(12)	287(15)	6.67(86)
C(415)	8319(6)	−1508(10)	1345(13)	5.81(73)
C(416)	8295(5)	−628(8)	2292(10)	4.15(60)
C(421)	8686(6)	1246(7)	4723(9)	3.58(53)
C(422)	9412(6)	1188(9)	4925(11)	4.60(63)
C(423)	9855(7)	1152(9)	5894(12)	5.22(71)
C(424)	9582(7)	1143(8)	6708(12)	5.48(70)
C(425)	8873(8)	1188(8)	6534(10)	4.80(70)
C(426)	8412(6)	1254(8)	5541(10)	4.12(63)

and $(PPN)_2$[**2b**] were made by the same method and with similar yields. IR (acetone, cm^{-1}) for $(PPN)_2$[**2a**]: 1980w, 1935s, 1845vs; for $(PPN)_2$[**2b**]: 1975w, 1930s, 1840vs; for $(PPN)_2$[**2c**]: 2008vw, 1966m, 1931s, 1855vs. Anal. Found: C, 64.83; H, 4.25; N, 1.83. $(PPN)_2$[**2a**] calc: C, 64.99; H, 4.06; N, 1.90%. Found: C, 63.28; H, 3.80; N, 1.71. $(PPN)_2$[**2b**] calc: C, 62.99; H, 3.94; N, 1.84%. Found: C,

59.97; H, 3.86; N, 1.41. $(PPN)_2$[**2c**] calc: C, 59.55; H, 3.75; N, 1.74%. Mössbauer spectrum for $(PPN)_2$[**2b**]: *IS*, −0.1199; *QS*, 1.12 mm s^{-1}; for $(PPN)_2$[**2c**]: *IS*, −0.11; *QS*, 1.34 mm s^{-1}.

Preparation of complexes (PPN)[(OC)$_4$Fe–E–Mo(CO)$_3$(η-C$_5$H$_5$)] (3) and (PPN)[(OC)$_4$Fe–E–W(CO)$_3$(η-C$_5$H$_5$)] (4)

Details of the synthesis of **3** apply also to **4**. A mixture of $(PPN)_2[(OC)_4Fe–Hg–Fe(CO)_4]$ (0.7 g, 0.43 mmol) and $[(\eta\text{-}C_5H_5)(OC)_3Mo–Hg–Mo(CO)_3(\eta\text{-}C_5H_5)]$ (0.3 g, 0.43 mmol) in THF (40 ml) was kept at room temperature then evaporated to half volume. Ether was slowly added to precipitate an orange solid, which was recrystallised from THF/hexane. Yield: 0.45 g, 92%. ^{1}H NMR ($CDCl_3$) for **3**: 5.39 (C_5H_5); for **4**: 5.40 (C_5H_5). IR (KBr, cm^{-1}) for **3**: 2005w, 1981m, 1962sh, 1937s, 1887s, 1859s, 1835s; for **4**: 2004w, 1979m, 1960sh, 1935s, 1885s, 1857s, 1833s. Anal. Found: C, 50.16; H, 3.10; N, 1.32. **3** calc: C, 50.04; H, 3.06; N, 1.22%. **4** calc: C, 46.49; H, 1.84; N, 1.13%. Found: C, 46.74; H, 2.72; N, 1.14.

Crystallographic section

Crystals of compound **2c** were grown from acetone/methanol (1/1). A prismatic crystal (0.07 × 0.07 × 0.1 mm) was mounted on a Philips PW-1100 four-circle diffractometer. The unit cell parameters were measured from 25 reflections ($4 \leq \theta \leq 12°$) and refined by least-squares method. Intensities were collected with graphite-monochromatized Mo-K_α radiation, using the ω-scan technique with scan width 0.8° and scan speed 0.03° s^{-1}. 5435 reflections were measured in the range $2 \leq \theta \leq 25°$, 5170 of which with $I \geq 2.5\ \sigma(I)$ were assumed as observed. Three reflections were measured every 2 h as orientation and intensity control, and no significant intensity decay was observed. Lorentz-polarization but not absorption corrections were made. *Crystal data*. $[C_{80}H_{60}N_2O_8P_4Fe_2Hg]$. $M = 1305.13$, triclinic, *a* 20.382(3), *b* 15.328(2), *c* 13.420(2) Å; α 115.96(3), β 108.89(2); γ 87.09(2)°. *V* 3546(1) Å^3, space group $P\bar{1}$, $Z = 2$, $D_c = 1.222$ g cm^{-3}, $F(000) = 1292$, Mo-K_α radiation (graphite monochromator), $\lambda = 0.71069$, μ(Mo-K_α) = 27.50 cm^{-1}, 288 K.

The structure was solved by direct methods, using the MULTAN system of computer programs [22] and refined by full-matrix least squares, using the SHELX76 program [23]. The function minimized was $\Sigma w[\,|F_o| - |F_c|\,]^2$, where $w = (\sigma^2(F_o) + 0.0034\,|F_o|)^{-1}$. *f*, *f′* and *f″* were taken from International Tables [24]. Positions of non-hydrogen atoms were refined anisotropically, and the positions of 48 hydrogen atoms were calculated. The final *R* value was 0.049 ($R_w = 0.053$) for all observed reflections. Max shift/e.s.d. = −0.4 in *x* of C(106). Max. and min. peak in final difference synthesis were 0.3 e Å^{-3} and −0.3 e Å^{-3}, respectively. The final positional parameters of the refined atoms are given in Table 2. Tables of all bond distances and angles, final hydrogen parameters, anisotropic thermal parameters, and a list of structure factors can be obtained from the authors.

Appendix

All molecular orbital calculations described in this paper were of the extended Hückel type [25] with modified Wolfsberg–Helmholtz formula [26]. The parameters used were taken from the literature [27] and are shown in Table 3.

Table 3

Orbital exponents (contraction coefficients of double-ζ expansion given in parenthesis) and energies used in the calculations

Atom	Orbital	ζ_i (c_i)	H_{ii} (eV)
C	$2s$	1.62	−21.4
	$2p$	1.62	−11.4
O	$2s$	2.27	−32.3
	$2p$	2.27	−14.8
Cl	$3s$	2.03	−30.0
	$3p$	2.03	−15.0
Fe	$4s$	1.90	−9.10
	$4p$	1.90	−5.32
	$3d$	5.35 (0.5366) 1.80 (0.6678)	−12.6
Hg	$6s$	2.65	−13.68
	$6p$	2.63	−8.47
Zn	$4s$	2.01	−12.4
	$4p$	1.70	−6.53

Calculations on $[(CO)_4Fe–M–Fe(CO)_4]^{2-}$ were carried out for M = Zn and Hg, assuming an eclipsed conformation (D_{3h} point group), except in the study of the conformational preference. All Fe–C bond distances were taken at 1.752 Å. Other bond distances used were: Fe–Hg = 2.523; Fe–Zn = 2.317; and C–O = 1.14 Å. MCO angles were kept fixed throughout at 180°. Test calculations including $5d$ orbitals for Hg gave the same qualitative results, and so we omitted those orbitals from subsequent calculations.

Acknowledgements

Financial support for this work was generously given by CICYT, through grants PB84-0920 (experimental work) and PB86-0272 (theoretical studies). The authors thank J. Tejada and J.R. Alabart for recording the ^{57}Fe Mössbauer spectra.

References

1 H. Behrens, H.D. Feilner, E. Lindner, D. Uhlig, Z. Naturforsch. B, 26 (1971) 990.
2 B.A. Sosinsky, R.G. Shong, B.J. Fitzgerald, N. Norem, C. O'Rourke, Inorg. Chem., 22 (1983) 3124.
3 L.W. Arnd, M.Y. Darensbourg, T. Delord, B.T. Bancroft, J. Am. Chem. Soc., 108 (1986) 2617 and references therein.
4 P.J. Krusic, D.J. Jones, D.C. Roe, Organometallics, 5 (1986) 456.
5 N.N. Greenwood, T.C. Gibb, Mössbauer Spectroscopy, Chapman and Hall, London, 1971, p. 223.
6 F.S. Stephens, J. Chem. Soc., Dalton Trans., (1972) 2257.
7 R.F. Bryant, H.P. Weber, Acta Cryst., Sect. A, 21 (1966) 138.
8 H.W. Baird, L.F. Dahl, J. Organomet. Chem., 7 (1967) 503.
9 G.M. Sheldrick, R.N.F. Simpson, J. Chem. Soc. (A), (1968) 1005.
10 B. Lee, J.M. Burlitch, J.L. Hoard, J. Am. Chem. Soc., 89 (1967) 6362.
11 R. Usón, A. Laguna, M. Laguna, P.G. Jones, G.M. Sheldrick, J. Chem. Soc., Dalton Trans., (1981) 366.
12 K.H. Whitmire, J.M. Cassidy, A.L. Rheingold, R.R. Ryan, Inorg. Chem., 27 (1988) 1347.

13 J. Silvestre, T.A. Albright, Isr. J. Chem., 23 (1983) 139.
14 (a) J. Silvestre, T.A. Albright, B.A. Sosinsky, Inorg. Chem., 20 (1981) 3937; (b) M. Elian, R. Hoffmann, Inorg. Chem., 14 (1975) 1058; (c) J.K. Burdett, J. Chem. Soc., Faraday Trans. 2, 70 (1974) 1599; (d) M.C. Böhm, J. Daub, R. Gleiter, P. Hofmann, M.F. Lappert, K. Öfele, 113 (1980) 3629; (e) R. Hoffmann, M.M.L. Chem, M. Elian, A.R. Rossi, D.M.P. Mingos, Inorg. Chem., 13 (1974) 2666.
15 R.H. Crabtree, M. Lavin, Inorg. Chem., 25 (1986) 805.
16 O. Rossell, M. Seco, I. Torra, J. Chem. Soc., Dalton Trans., (1986) 1011.
17 M.J. Mays, J.D. Robb, J. Chem. Soc. (A), (1968) 329.
18 F. Bonati, S. Cenini, R. Ugo, J. Chem. Soc., (A), (1967) 932.
19 F.G.A. Stone, Angew. Chem., Int. Ed. Engl., 23 (1984) 89.
20 O. Rossell, M. Seco, P. Braunstein, J. Organomet. Chem., 273 (1984) 233.
21 M.Y. Darensbourg, D.J. Darensbourg, H.L.C. Barros, Inorg. Chem., 17 (1978) 297.
22 P. Main, S.L. Fiske, S.E. Hull, J.P. Germain, J.P. Declercq, M.M. Woolfson, MULTAN, System of computer programs for crystal structure determination from X-ray diffraction data; University of York, University of Cambridge, 1976.
23 G.M. Sheldrick, SHELX, a computer program for crystal structure determination. University of Cambridge, 1976.
24 International Tables of X-ray Crystallography, Kynoch Press: Birmingham, 1974, pp. 99–100 and 149.
25 R. Hoffmann, J. Chem. Phys., 39 (1963) 1397.
26 J.H. Ammeter, H.-B. Bürgi, J.C. Thibeault, R. Hofmann, J. Am. Chem. Soc., 100 (1978) 3686.
27 (a) R.H. Summerville, R. Hoffmann, J. Am. Chem. Soc., 98 (1976) 7240. (b) D.J. Underwood, M. Novak, R. Hoffmann, J. Am. Chem. Soc., 107 (1985) 5968.
28 C.G. Pierpont, B.A. Sosinsky, R.G. Shong, Inorg. Chem., 21 (1982) 3247.
29 R.J. Neustadt, T.H. Cymbaluk, R.D. Ernst, F.W. Cagle, Inorg. Chem., 19 (1980) 2375.